BIOCHEMICAL AND BIOPHYSICAL RESEARCH COMMUNICATIONS **246,** 261–266 (1998)
ARTICLE NO. RC988594

Fine Profile of Actomyosin Motility Fluctuation Revealed by Using 40-nm Probe Beads

Haruto Nakayama, Takako Yamaga, and Yuki Kunioka
Kansai Advanced Research Center, Communications Research Laboratory, Iwaoka 588-2, Nishi-ku, Kobe 651-2401, Japan

Received April 3, 1998

The displacement of colloidal gold beads only 40 nm in diameter can be detected with spatial and temporal resolutions of 2.8 nm and 0.5 msec by using an optical setup in which two laser beams are reflected on the same field of a prism surface, forming interference fringes in an evanescent field adjacent to the prism surface, and the changes in scattering intensity that occur when the beads move across the fringes are measured in optical microscopic images. Results obtained when using this setup and actin-bound gold beads to measure the movement of actin filaments on myosin motor molecules revealed the fine profile of movement fluctuation and that the duty time of a single stroke of myosin motors is less than 10-20 milliseconds.

Key Words: **nanometric measurement; 40-nm-diameter colloidal gold beads; actomyosin motility assay; evanescent light field.**

Since a method for measuring the nanometer-order displacement of small beads under optical microscopes was developed (1), many important characteristics of biological molecules have been revealed at the level of single molecules (2,3). The minimum size of the beads used in this method, however, has been only of submicrometer order (4) and has limited the temporal resolution, whereas size of single biological molecules ranges from a few nanometers to a few tens of nanometers. The movements of such large beads thus does not directly represent the movements of single molecules: the large surface area of the beads near the attached molecules can give rise to artifacts by interacting with the basement surface, in the measurement of piconewton-order forces the viscous resistance in a solution results in low temporal resolution (5) regardless of the temporal resolution of sensor circuits, the movement of a single molecule is limited by the steric hindrance due to micron-size beads, and rotation of probe beads cancels the displacement of beads effected by the attached motor proteins in the case of nonunidirectional movement like rotation or vibration. These limitations can be overcome by using probe beads of nanometer-order size. Nanometer-size beads have been used to measure nanometer-order displacements of particles in the cell surface (6), but the temporal resolution of that method is not better than 33 milliseconds, whereas a temporal resolution of a millisecond or better is required in order to reveal the dynamics of the function of a single molecule (7, 8).

The main obstacle to the application of nanometer-size beads has been the weak scattering intensity of the beads, which results in a low contrast image with a small S/N ratio. In this report we combine the conventional optical microscope with an evanescent-dark-field illumination produced by laser beams (9, 10, 11) in order to assure a stable and strong illumination field and images of high contrast, and with two-beam interference fringes (12) in order to detect displacement in relatively low-intensity images. This system could detect the movement of gold beads 40 nm in diameter with a spatial resolution smaller than 3 nm and with a temporal resolution of 0.5 msec. Using this system to investigate actomyosin sliding movement, we were able to observe the fine structure of motor strokes.

MATERIALS AND METHODS

1. Motility assays. All chemicals except for phalloidin-rhodamine were purchased from Sigma Co. and were of special grade. Phalloidin-rhodamine was purchased from Molecular Probe Inc. Protein preparation and the motility assay were as described as Harada et al. (13) except that the chymotriptic S1 fragment instead of myosin was used in motility assay. Colloidal gold beads were bound to actin filaments through gelsolin.

2. Experimental setup. The experimental apparatus is shown schematically in Fig. 1. All optical mounting components were, if not specified otherwise, from Sigma Koki Co. (Tochigi, Japan). The 514-nm light beam from the Ar ion gas laser (model 2020, Spectra Physics, USA) was passed through a condenser lens (f = 400 mm) and then split into two beams of equal intensity by a beam-splitter. Between the laser head and the beam-splitter, the beam was steered by two mirrors, and consequently the p-plane polarized light was converted into s-plane polarized light. After one of the two beams was reflected, they entered a quartz prism fixed on the sample stage

0006-291X/98 $25.00

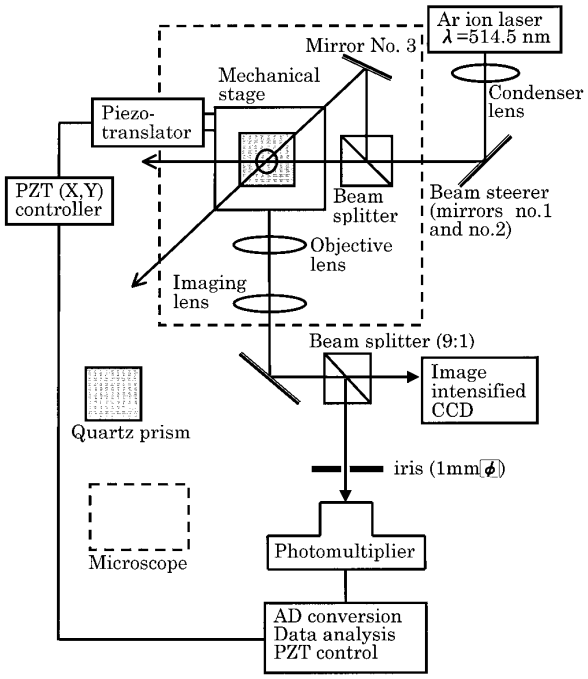

FIG. 1. Schematic of the custom-built microscope system.The top view is shown for the components from the laser to the specimen, and a side view is shown for the components from the objective lens to the photomultiplier/CCD videocamera. The components shown within the dashed box were firmly fixed with respect to each other by being mounted on a hand-made metal block. The circle in the center of the shadowed box (quartz prism) represents the specimen area, where evanescent light field fringes are formed. Details are described in Materials and Methods.

of an optical microscope and crossed at the lower surface of the prism with the crossing angle of 0.162 radian. The angles at which each of the beams was incident to the prism/water interface was adjusted as follows: the angle was first set precisely at the critical angle by examining the transmitted leak light, and then the position of mirror No.2 was shifted slightly by an amount corresponding to an increase of the incident angle by $<8.7 \times 10^{-4}$ radian. The sample solution was placed under the lower prism surface, sandwiched by a 0.17-mm-thick cover glass, and observed by using an inverted optical microscope (Zeiss, Axiovert 100) equipped with a Neofluor 100 objective lens (NA 1.30). The sample stage had been replaced with a mechanical stage (Σ212S, Sigma Koki) equipped with piezo-actuators (P-249.10, Physik Instruments) for both the X and the Y directions. The noise due to mechanical vibration was reduced by mechanically separating from the microscope all of the optical components after imaging lens. All optical components, including the laser head, were fixed on an air-damped optical bench. Specially, the basement for the mechanical stage and objective lens of the microscope was replaced with a large aluminum block (about 200 × 200 × 150 mm), and this block, the beam splitter, and the mirror after the beam splitter (mirror No. 3), were firmly fixed to each other by many 20-mm-thick brass and aluminum bars.

3. Signal detection. Ninety percent of the light in the beam from the sample was directed to a photomultiplier (R374, Hamamatsu Photonics, Hamamatsu) through a circular iris settled on the imaging surface. The 1-mm diameter of the iris corresponded to a diameter of 7 μm at the sample. The output current of the photomultiplier was amplified and frequency-filtered, digitized by an AD converter (ADXM-98A, Canopus, Kobe) after amplification (C1556-50, Hamamatsu Photonics) and frequency filtration (ASIP-0260, Canopus), and then stored in and analyzed by a personal computer (PC9800, NEC, Japan). The ten percent of the sample beam not directed to the photomultiplier was monitored by an image-intensified CCD videocamera (2400-08, Hamamatsu Photonics, Shizuoka).

RESULTS AND DISCUSSION

If the position of a bead is to be determined with a resolution of nanometer order, the intensity of illuminating light should be temporally stable and spatially homogeneous. Interference fringes of the evanescent field were visualized by illuminating a concentrated solution of rhodamine B (Fig. 2). Uniform stripes are seen with very high contrast (max/min intensity ratio is typically 8.5). Positional stability of the stripes depended mainly on the constancy of the relative positions of three optical components: the beam splitter, mirror No. 3, and the prism. Stabilizing these elements limited the fluctuation due to mechanical instability to the frequencies lower than a few hertz (14). The size of illumination area was controlled to about 60 × 200 μm by using the condenser lens to adjust the position of focus of the laser beams, and the intensity of the stripes was uniform over the field of interest for a single measurement (about 10 × 10 μm). The temporal stability of the intensity of the illuminating light depended mainly on the laser intensity stability and pointing stability. Careful tuning of the laser and making the distance from laser head to the sample prism as short as possible (450 mm) kept the illumination intensity stable. The spatial periodicity of the stripes can be controlled by changing angle at which the two incident beams cross (12). The larger this angle, the narrower the stripe spacing. This results in higher contrast until the spacing approaches the wavelength, when contrast decreases because of the effect of the diffraction limit (9). Measuring the contrast while changing the crossing angle, we found that the crossing angle corresponding to a periodicity of 1.32 μm would result in fringes with the highest contrast. The thickness of the evanescent field depends on the angle at which the beam is incident to the interface: larger angles give thinner fields (12). In the present study the incident angle was set at 1.13 radians in order to get the thickest field possible (see Materials and Methods; the field intensity decays to 1/e at >1.4 μm) because for the present study the scattering intensity of a bead should not be sensitive to sample movement perpendicular to the prism surface.

When we illuminated the aqueous solution of colloidal gold beads 40 nm in diameter (EM grade, Zymed Laboratories, California, USA), only surface attached beads are clearly seen (Fig. 3). Background light was mainly from dim images of surface disorder of the prism surface. The image intensity was higher than that of the beads visualized by a differential interference contrast microscope, but was still not high enough

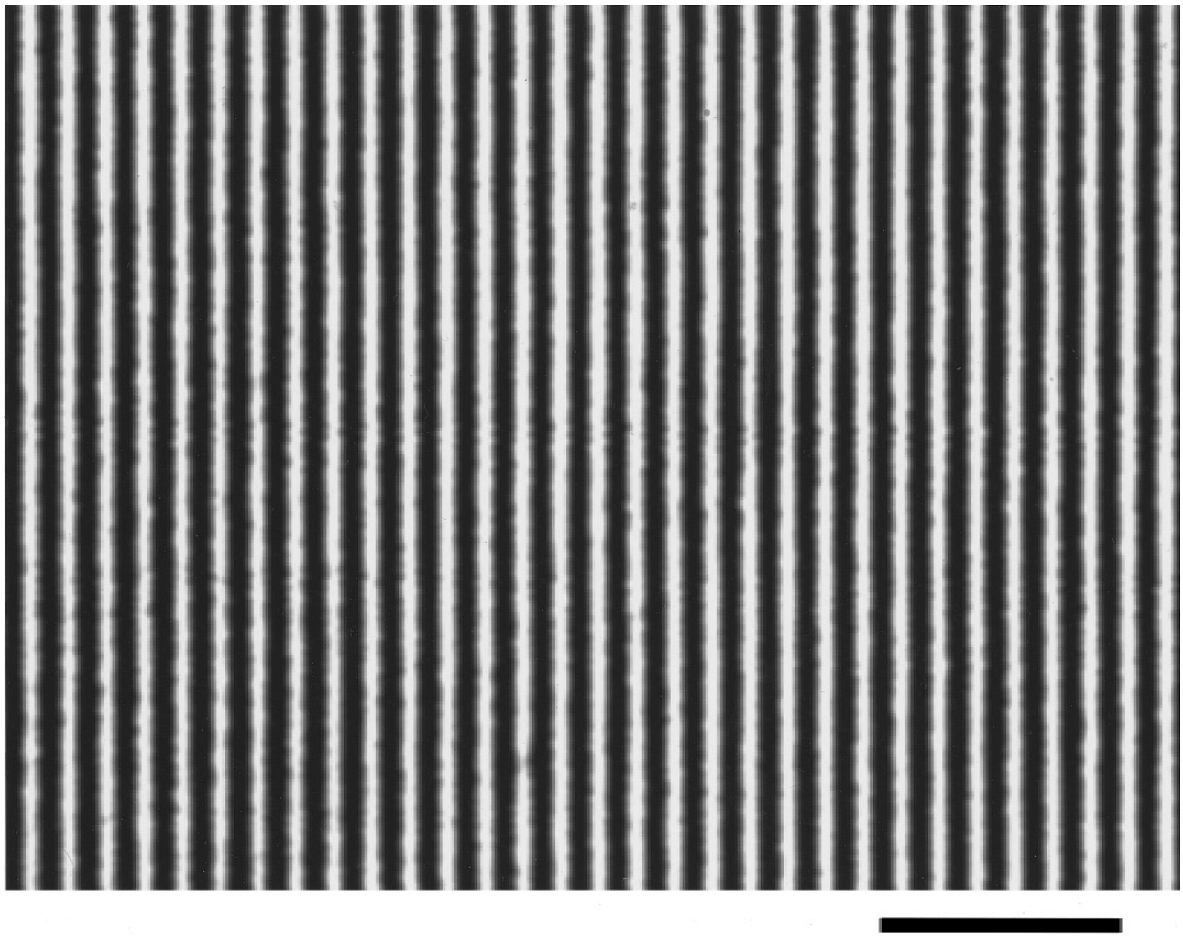

FIG. 2. Interference fringes of the evanescent field.The sample space was filled with an aqueous solution of rhodamineB and illuminated by the evanescent field light produced by two crossing laser beams (green, λ=514 nm). Green-cut barrier filter was set after objective lens to pass only rhodamineB fluorescence and a fluorescence image of high-contrast stripes could be visualized as a result of interference fringes of excitation light. Beams are from upper right to the lower left and from the upper left to the lower right. The period of the fringes is 1.32 μm (corresponding to a crossing angle of 0.162 radian). Eight consecutive image frames of a video record from the CCD camera were digitized and averaged. (Bar: 10 μm).

to be detected quantitatively by quadrant-type photodiodes. In contrast to the images from conventional dark-field microscope (15), the images are essentially free of background noise originating from leakage of the incident light and unstable scattering by floating out-of-focus beads. Image intensity of the beads varied from one bead to another because the intensities with which the beads were illuminated depended on the position relative to the intensity peaks of the fringe. The apparent size of the bead image was about 0.4 μm. Such small images cannot be detected effectively by a quadrant photodiode, which has insensitive area at the center of the sensor surface. Because the shapes of the images are not always of circular symmetry, it is difficult to find a proportionality between the displacement and intensity ratio when a quadrant-photodiode detector is used. Transmission-electron-microscopic observation confirmed that the beads were largely free from aggregation and that practically all beads seen were single beads.

The iris in front of the photomultiplier limited the background light (see Fig. 1), and intensity measurement of a bead without interference fringes revealed that the illumination-intensity fluctuation due to the laser itself and to pointing instability was less than 0.2%. When we moved a surface-attached bead across the fringe by shifting the stage in one direction, the intensity of the bead image changed periodically (Fig. 4(a)). The shape and the period of the intensity change was the same as that of the fringe pattern (Fig. 2), showing that the image intensity well represents the position of the beads on the fringe. The gradient is steepest midway between an intensity maximum and minimum, and this area was therefore chosen as a data acquisition area because there the changes in bead intensity are most sensitive to the displacement.

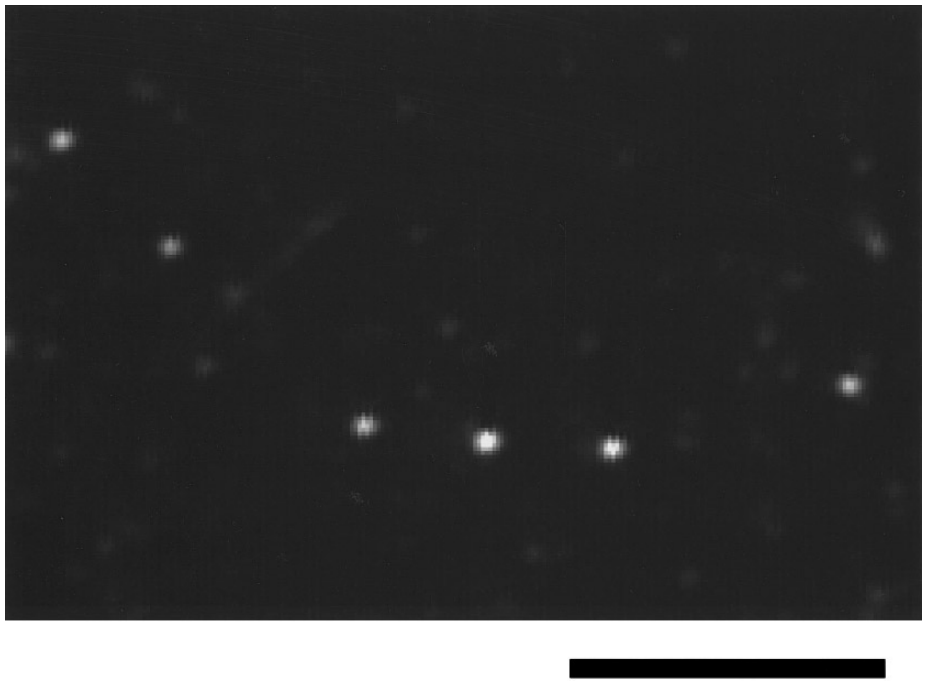

FIG. 3. Images of beads 40 nm in diameter visualized by the scattering of evanescent field light. Aqueous solution of colloidal gold beads 40 nm in diameter was illuminated by evanescent field fringes. The green-cut barrier filter was not set to the microscope and scattered light was used to form images. An image of accidentally surface-attached beads was recorded by the CCD camera, and eight consecutive frames from a video record were digitized and averaged. (Bar: 10 μm).

The intensity change in this region is enlarged and shown in Fig. 4(b). The regression curve for the data in Fig. 4(b) is close to a straight line, showing that the relation between image intensity and displacement is linear within this roughly 200-nm range. The gradient of the regression line is 0.012 V/nm, and the root mean square of the deviation from the line is 0.034 V. Therefore, the spatial resolution of this displacement-measurement system is 2.8 nm (0.034/0.012). The temporal resolution of the measurement apparatus was 0.1 msec. When we tried using the system to visualize smaller particles (20 nm in diameter), we obtained images of dots, but the images were too faint to be used in making nanometer-order measurements.

We used this system to investigate actin-myosin sliding in an attempt to observe the fine profile of process generating force. Beads 40 nm in diameter were bound to actin filaments through gelsolin and were slid on myosin heads bound to the glass surface. Sliding movements of rhodamine-stained actin filaments could be visualized by inserting a barrier filter for rhodamine fluorescence after objective lens. Filaments with and without bound beads slid similarly, and no disorder or immediate stop of the movement after the start of illumination was observed. Direction of the sliding movements was at random. Only movements perpendicular to the fringe stripes were chosen and subjected to the nanometer-scale measurement.

Trace (a) in Fig. 5 shows the displacement of a bead fixed to the surface through F-actin-myosin in rigor. There was no net displacement over a long period ($>$100 milliseconds). Fine noise with a frequency near that corresponding to the temporal resolution (2 kHz) can be seen, but there is no evident fluctuation at lower frequencies. Traces (b) to (d) show the movement of the F-actin-bound beads. Because the fine noise can be seen in all the traces in Figs. 4 and 5 (including that of a fixed bead), it is evidently due to the measurement system. The effect of the movement perpendicular to the glass surface was estimated by switching off one of the two incident beams. The output signals obtained without interference fringes (one incident beam off) were constant over the long term and contained homogeneous noise similar to that in the signals from surface-bound beads (Fig. 5(a)). This indicates that movement perpendicular to the surface does not affect the output signal. The traces of the beads bound to the sliding F-actin (Figs. 5(b) to 5(d)) contain slow fluctuations which is not seen in the trace of a fixed bead (Fig. 5(a)): fluctuations with a time-width of 10-20 milliseconds and an amplitude of 5-10 nm are evident in Figs. 5(b)-5(d). These fluctuations are presumably due to myosin motor strokes. Because a bead-bound F-actin filament can be affected by many motor molecules at given time, the movement of a bead bound at the edge of F-actin filament should be a result of overlaps of strokes

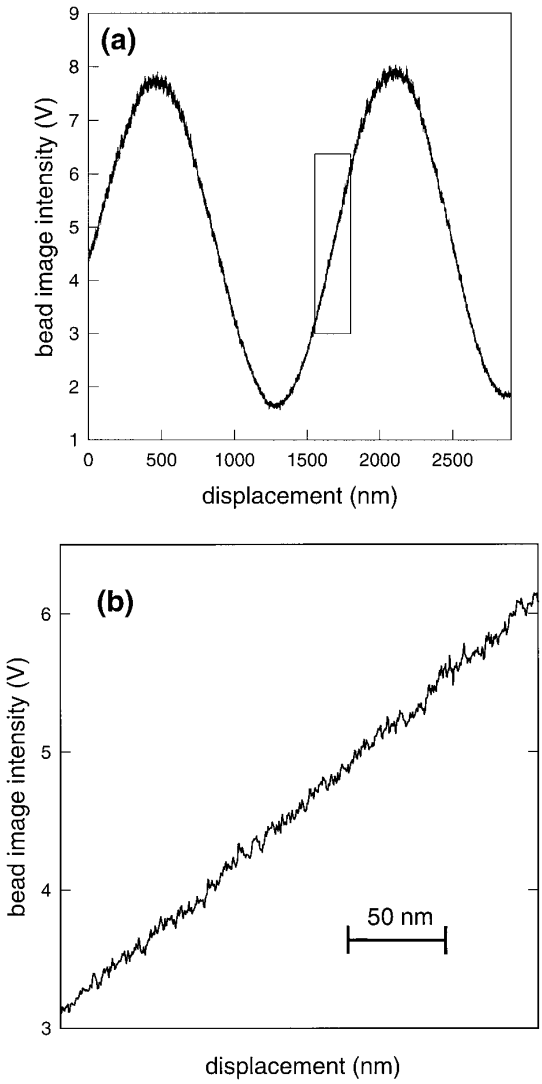

FIG. 4. Representative displacement trace of a bead firmly attached to the prism surface.(a) Beads were attached to the prism surface by adding 50mM NaCl. The piezotranslator was used to move the bead in one direction by shifting the stage 2 μm/sec so that the image crossed the area corresponding to the iris in front of the photomultiplier. Shown is an intensity change for a bead moving perpendicular to the fringe stripes. Bandwidth: 2 kHz. Displacement was calibrated by estimating the positions of scalar images which was shifted by the piezotranslator that shifted the stage. (b) Enlarged display of a portion of the trace in Fig. 4. A portion with the steepest gradient was chosen from the trace in Fig. 4 (box mark in the center of Fig. 4(a)) and enlarged. Straight line: line fitted to the trace.

of motor molecules (at least a few adjacent ones). The temporal resolution of the displacement-measuring apparatus is fine enough to resolve the profile of the fluctuation, and because the beads are extremely small the profile reflects the effect of motor molecules directly without the effect of viscous resistance. In general averaging due to overlap of peaks having definite width and amplitude usually results in peaks of larger width and lower amplitudes than the original peaks (16). Because the observed peak profiles are the result of the averaging due to the overlap of single strokes of myosin motors, the profile of the original single stroke should have shorter time duration and longer amplitude (step size); that is, $<$10-20 milliseconds and $>$5-10 nanometers. Recent studies have developed motility-assay sample systems that can be used to observe single strokes of motor molecules (7,8), and reported the size of single strokes without enough temporal resolution to argue the detailed profile of a single stroke. Application of our microscope system to these sample systems should be able to reveal the fine profile of single strokes without the affection of overlaps.

It is essential for the understandings of the molecular mechanism of biological motor to observe how pro-

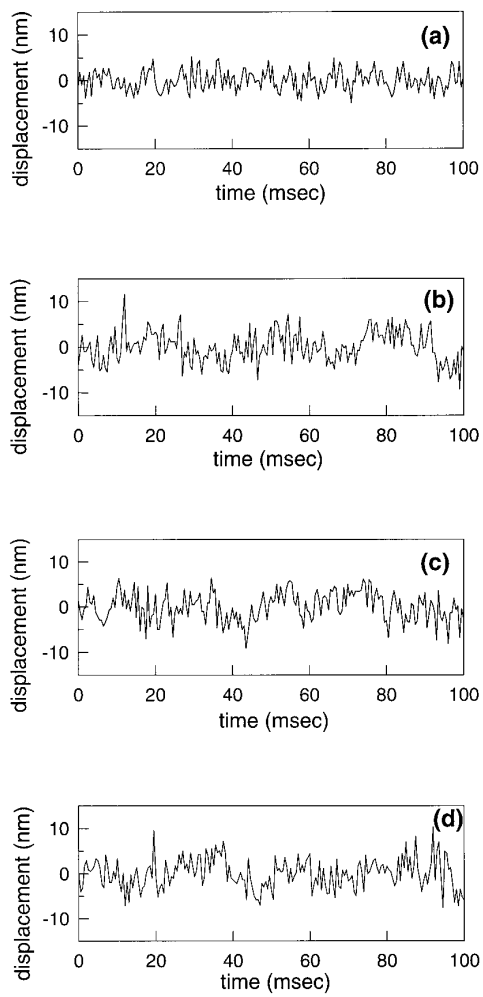

FIG. 5. Movement fluctuation of actomyosin motility. Time-dependent displacement of beads bound to F-actin in a motility assay is shown. Bandwidth is 2 kHz. (a) Trace of a bead bound to the surface through myosin-bound F-actin in rigor. (b) to (d) representative traces of beads bound to F-actin in active sliding motion. For clarity of presentation, a straight line fitted to the original data was subtracted from the data. What are shown are the resultant traces of fluctuation.

files of single strokes change under an external load. Our microscope system have enough open space to insert new optical components (Fig. 1) and can be equipped with laser-tweezers optics that we could use to measure molecular forces and to load molecules with an external force. It has been shown that 40-nm colloidal gold beads can be captured by a laser-tweezers system (17).

Our measurement system is especially powerful for investigating the nonunidirectional movement like rotation. The rotation of bacterial flagellar motor (18) or F_1-ATPase (19) was observed by using bacterial flagella or F-actin as probes. When applied to those samples, our measurement system should be able to reveal more intact details of function, because it does not request such large probes.

ACKNOWLEDGMENTS

The authors thank Drs. Kazuhiro Oiwa and Hiroaki Kojima, also at the Kansai Advanced Research Center, for valuable discussions.

REFERENCES

1. Kamimura, S. (1987) *Appl. Optics* **26,** 3425–3427.
2. Kishino, A., and Yanagida, T. (1988) *Nature* **334,** 74–76.
3. Svoboda, K., Schmidt, C. F., Schnapp, B. J., and Block, S. M. (1993) *Nature* **365,** 721–727.
4. Malik, F., Brillinger, D., and Vale, R. D. (1994) *Proc. Natl. Acad. Sci. USA* **91,** 4584–4588.
5. Svoboda, K., and Block, S. M. (1994) *Annu. Rev. Biophys. Biomol. Struct.* **23,** 247–285.
6. Kusumi, A., Sako, Y., and Yamamoto, M. (1993) *Biophys. J.* **65,** 2021–2040.
7. Finer, J. T., Simmons, R. M., and Spudich, J. A. (1994) *Nature* **368,** 113–119.
8. Ishijima, A., Harada, Y., Kojima, H., Funatsu, T., Higuchi, H., and Yanagida, T. (1994) *Biochem. Biophys. Res. Commun.* **199,** 1057–1063.
9. Borm, M., and Wolf, E. (1975) Principles of Optics, Pergamon Press, London.
10. Axelrod, D. (1989) *Meth. Cell Biol.* **30,** 246–270.
11. Oiwa, K., Anson, M., Yamada, A., Eccleston, J. F., Corrie, J. E. T., Ferenczi M. F., Trentham, D. R., and Nakayama, H. (1996) *Biophys. J.* **70,** A159.
12. Abney, J. R., Scalettar, B. A., and Thompson, N. L. (1992) *Biophys. J.* **61,** 542–552.
13. Harada, Y., Sakurada, K., Aoki, T., Thomas, D. D., and Yanagida, T. (1990) *J. Mol. Biol.* **216,** 49–68.
14. Li, D., and Schnapp, B. J. (1996) *Rev. Sci. Instr.* **68,** 2195–2199.
15. Horio, T., and Hotani, H. (1986) *Nature* **321,** 605–607.
16. Ishijima, A., Doi, T., Sakurada, K. and Yanagida, T. (1991) *Nature* **352,** 301–306.
17. Svoboda, K., and Block, S. M. (1994) *Optics Letters* **19,** 930–932.
18. Kudo, S., Magariyama, Y., and Aizawa, S. (1990) *Nature* **346,** 677–680.
19. Noji, H., Yasuda, R., Yoshida, M., and Kinosita K., Jr. (1997) *Nature* **386,** 299–302.